AIAA 2016-4325

AIAA Aviation
13-17 June 2016, Washington, D.C.
34th AIAA Applied Aerodynamics Conference

# Evaluation of Reduced-Order Models for Predictions of Separated and Vortical Flows

Ryan Darragh* and Peter E. Hamlington†

*Department of Mechanical Engineering, University of Colorado, Boulder, CO 80309*

Mehdi Ghoreyshi‡ and Andrew J. Lofthouse§

*High Performance Computing Research Center, U.S. Air Force Academy, CO 80840*



**Computational fluid dynamics (CFD) simulations have the potential to provide predictions of flow around airfoils and wings of arbitrary complexity, without the need to perform real-world testing and experimentation. However, the computational cost of such simulations increases dramatically as the complexity of the modeled geometry increases, thus imposing limitations on the use of CFD for design optimization where many different flight conditions must be considered. Reduced-order models can overcome these limitations by providing rapid calculations of the flow field at a fraction of the computational cost, but the accuracy of such models can be substantially reduced in flows with complex physics, such as flow separation. In this paper, we compare the accuracy of three reduced-order models for calculating the coefficient of pressure, $C_p$, on both simple (i.e., NACA0012 airfoil) and complex (i.e., NACA64A006 wing) aerodynamic configurations at different angles of attack, including high angles of attack where flow separation occurs. These models are trained using CFD data and the capability of the models to predict $C_p$ for new angles of attack is characterized. We find that reduced-order models based on local interpolation methods are the most accurate, although the accuracy becomes worse overall for a three-dimensional wing and worse in particular for high angles of attack where flow separation occurs.**

## I. Introduction

Aircraft design optimization requires an understanding of the interactions between flow fields – which are often unsteady, separated, and turbulent – and aerodynamic structures such as airfoils or wings. Although these interactions can be studied using reduced-scale physical models in wind tunnels, a cheaper and faster alternative is to numerically model the flow using computational fluid dynamics (CFD) simulations. Such simulations allow a broader range of design parameters to be tested than is experimentally feasible, typically in a much shorter span of time. However, CFD simulations can be prohibitively expensive for realistic geometries, even using Reynolds-averaged Navier-Stokes (RANS) approaches. This is particularly true when a wide range of flight conditions, such as different angles of attack, must be considered.

The significant cost of performing many full CFD simulations has motivated the creation of reduced-order models. These models are commonly used as a reduced-cost approach to predict aircraft flow fields at different flight conditions. In contrast to CFD, reduced-order models do not involve the solution of physics-based governing equations, and instead use known experimental and CFD results as "training data" to empirically relate aerodynamic properties such as the coefficient of pressure, $C_p$, to flight conditions, such as the angle of attack. When considering a broad range of continuous flight conditions, building such models can be much simpler than performing an essentially limitless series of CFD simulations, given that the speed of reduced-order models is almost instantaneous when compared to typical CFD codes. The simplicity

*Graduate Student, Aerospace Engineering Sciences, ryan.darragh@colorado.edu, AIAA Student Member
†Assistant Professor, Mechanical Engineering, peter.hamlington@colorado.edu, AIAA Member
‡Senior Aerospace Engineer, mehdi.ghoreyshi.ctr.gb@usafa.edu, AIAA Senior Member
§Director, High Performance Computing Research Center, andrew.lofthouse@usafa.edu, AIAA Senior Member

and speed of these models also introduces the possibility of improved real-time flight control and stability. However, the accuracy of reduced-order models can suffer as a result of not directly solving physics-based flow equations. This is particularly true when a flow undergoes a "regime change," such as occurs during flow separation at high angles of attack. As a result, any practically-useful reduced-order model must not only be fast, but must also correctly predict the response of aerodynamic systems for a wide range of flight conditions.

A common reduced-order modeling approach is the "table-lookup" method,[1–3] which requires the tabulation of large amounts of data at various flight conditions and the interpolation of known tabulated values to determine unknown values. However, as modern interpolation, mode decomposition, and machine learning methods have been developed, the accuracy and complexity of reduced-order models has improved. Kriging[1,3–5] and Cokriging[2,6–8] methods, in particular, have been widely used recently to create reduced-order models for various aerodynamic problems using tabulated data of varying complexity, including results from CFD. Motivated by the nonlinearity and complexity of flow field data that must be represented by reduced-order models, nonlinear Volterra series[9,10] and linear convolution models with nonlinear corrections[11] have also been investigated for the prediction of unsteady aerodynamic loads. More recently, the use of mode decomposition methods such as radial basis functions[10] and proper orthogonal decomposition[12] have been used to represent complex flow fields and aerodynamic responses with relatively few degrees of freedom. Lillian *et al.*[12] used POD, and singular value decomposition (SVD) in particular, with CFD training data to predict the surface pressures on an F-16 wing.

In many cases, the development of reduced-order models has been posed as a "system identification" problem,[13] on which many modern machine learning methods can be brought to bear. For example, artificial neural networks have been created to model the lateral and longitudinal responses of an aircraft in order to develop a control system[14] and to model aircraft response over wide ranges of angle of attack.[15] Similarly, support vector machines have been used to capture the complicated flow generated at high angles of attack by complex aerodynamic geometries.[16] In general, interpolation, mode decomposition, and machine learning methods have all resulted in reasonably accurate reduced-order models, and work continues to improve their overall capabilities.[17] Other methods for developing reduced-order models include the method of segments, which has been used in high Mach number regimes,[11] and the auto-regressive moving average method to deal with airfoil gust responses.[18] A number of these methods have been compiled together into a single software packaged called System Identification Programs for Aircraft (SIDPAC).[19] This package includes a wide range of software to meet many system identification needs, and often serves as a baseline against which new methods are tested.

In the present paper, we are specifically focused on the development of reduced-order models for both simple and complex aerodynamic configurations at different angles of attack, including high angles of attack where flow separation occurs. We consider three different reduced-order models, including (*i*) SVD, which is a global method inspired by the work of Lillian *et al.*,[12] (*ii*) localized SVD, which is designed to increase the locality of the SVD interpolation, and (*iii*) the Kriging method,[1,3–5] which is a local interpolation method. These models are each "trained" here using data from a series of CFD simulations that solve the steady RANS equations in order to obtain the coefficient of pressure, $C_p$, at different angles of attack. The resulting models are then tested at new angles of attack for both simple (i.e., the NACA0012 airfoil) and complex (i.e., the NACA64A006 wing) geometries, revealing that model accuracy depends on the complexity of the geometry as well as on whether the flow has separated. Our particular interest is in determining whether a single reduced-order model can accurately predict aerodynamic loads across a wide range of flight conditions (i.e., angles of attack) during which the flow transitions from a largely attached to a massively separated behavior, with a specific focus on the relative accuracies of local versus global interpolation methods.

In the following, a description of the CFD simulations is provided first, followed by an outline of the three reduced order models used in this study. Results are then presented and a discussion and conclusions are provided at the end.

## II. Description of Numerical Simulations

Training data for the development of the three reduced-order models considered here is obtained from numerical simulations performed using the CFD code COBALT,[20] which is a parallelized finite volume flow solver capable of resolving flow over complex geometries using both structured and unstructured grids in two or three dimensions (2D or 3D, respectively). COBALT solves the compressible RANS equations with up

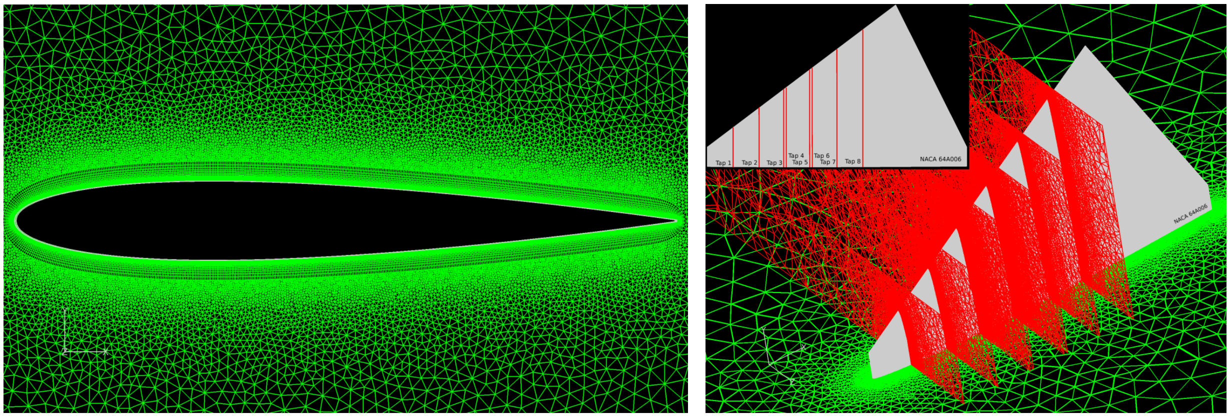


(a) NACA0012 grid

(b) NACA64A006 grid with tap positions

Figure 1: Computational grids for (a) the two-dimensional NACA0012 airfoil[21] and (b) the three-dimensional NACA64A006 wing.[22] Panel (b) includes eight planes (or "taps") in red where we measure $C_p$ over the wing. The inset shows a profile view of these planes. Note that a peniche is included below the NACA64A006 wing to mimic the experimental setup Hövelmann *et al.*[23]



to second order spatial and temporal accuracy. It uses Godunov's first-order accurate, cell-centered, finite volume, exact Riemann solution method. A variety of flow data are output from COBALT, including velocity and vorticity fields, as well as pressure at user-specified tap locations.

Using COBALT, we solve the steady RANS equations for the NACA0012 airfoil[21] and the NACA64A006 wing[22] at various angles of attack. All simulations for both geometries are performed using second order spatial accuracy and an ideal gas equation of state. The 2D NACA0012 unstructured grid is shown in Figure 1(a) and the 3D NACA64A006 unstructured grid is shown in Figure 1(b). The geometry for the NACA64A006 case includes a peniche, mimicking the experimental configuration studied by Hövelmann *et al.*[23] A total of 70198 grid cells[24] are used for each of the NACA0012 simulations and 13.2 million grid cells[25] are used for each of the NACA64A006 simulations. The Spalart-Allmaras rotation corrected (SARC) RANS model is used for both cases with second-order spatial accuracy.

Steady state flow fields are computed for both the NACA0012 airfoil and the NACA64A006 wing at various fixed angles of attack, where the incoming flow speed is Ma=0.15 in all cases (this flow speed matches the experimental conditions of Hövelmann *et al.*[23]). The simulations for each angle of attack were run on Cray XE6 (Garnet, 2.5GHz) and Cray XE6m (Copper, 2.3GHz) supercomputers for approximately 3600 CPU hours over 256 CPUs. In all cases, 6000 iterations were required in order to reach a steady state condition. Data is obtained by varying only the angle of attack in each simulation and keeping all other parameters the same. We simulated angles ranging from 0° to 20° for the NACA0012 and 1° to 21° for the NACA64A006. The specific selection of angles is described in Section III.D.

In order to obtain $C_p$ values on the 3D NACA64A006 wing, pressure measurement "taps" are placed at eight locations along the span of the wing, as shown in Figure 1(b). Tap locations are identical to the measurement locations in the experiment of Hövelmann *et al.*[23] and consist of planes at $x/c = \{$ 0.12, 0.24, 0.354, 0.366, 0.474, 0.486, 0.600, 0.72$\}$, where $c$ is the chord length, which varies along the span of the wing. For the 2D NACA0012 case shown in Figure 1(a), $C_p$ values are taken along the surface of the airfoil.

## III. Description of Reduced Order Models

The reduced-order models considered here involve the construction of an interpolating function using known values of $C_p$ at a range of angles of attack, $\alpha$. Interpolation methods can be categorized in a few different ways, but of greatest interest here are those that are global versus those that are local. Global methods take into account all of the information from a given range of input conditions. This causes these methods to act as though they are averaging the data, and thus they tend to produce better results when extreme values must be neglected. On the other hand, local methods only take into account information from data near the condition of interest, causing them to better reproduce local characteristics of the function they are interpolating, such as minima or maxima. In the following, we briefly describe the SVD method, which is a global method, and the localized SVD and Kriging methods, both of which are local methods.

### A. Singular Value Decomposition

Singular value decomposition (SVD) is a matrix method that decomposes data into singular values and vectors. We implement the method of Lillian *et al.*[12] on our matrix of $C_p$ values at each angle of attack $\alpha$ and each tap location $(y, x)$. We begin with an $A$ matrix for a given tap, $x_0$, where we want to create a model out of $n$ angles of attack $\alpha$. Our matrix would then be

$$A_{x_0} = \begin{bmatrix} C_p(\alpha_0, y_0, x_0) & C_p(\alpha_1, y_0, x_0) & \dots & C_p(\alpha_n, y_0, x_0) \\ C_p(\alpha_0, y_1, x_0) & C_p(\alpha_1 y_1, x_0) & \dots & C_p(\alpha_n, y_1, x_0) \\ \vdots & \vdots & \ddots & \vdots \\ C_p(\alpha_0, y_m, x_0) & C_p(\alpha_1, y_m, x_0) & \dots & C_p(\alpha_n, y_m, x_0) \end{bmatrix}. \tag{1}$$

We then decompose $A_{x_0}$ using SVD into $A = U\Sigma V^T$ where $U$ and $V$ are the left and right singular vectors and $\Sigma$ is the matrix of singular values. Next, we introduce

$$R = \begin{bmatrix} \alpha_0^0 & \alpha_0^1 & \alpha_0^2 & \dots & \alpha_0^M \\ \alpha_1^0 & \alpha_1^1 & \alpha_1^2 & \dots & \alpha_1^M \\ \vdots & \vdots & \vdots & \ddots & \vdots \\ \alpha_n^0 & \alpha_n^1 & \alpha_n^2 & \dots & \alpha_n^M \end{bmatrix} \tag{2}$$

where $M \in \mathbb{N}$ is the maximum order to which we expand. For the present analysis, we use $M = 3$. We then solve for a matrix of coefficients $C$ such that $RC \approx V$. Returning to our $A_{x_0}$ matrix, we have

$$A = U\Sigma V^T = U\Sigma(RC)^T = U\Sigma C^T R^T. \tag{3}$$

We can now interpolate to obtain $C_p$ values at $l$ new angles of attack by defining

$$\tilde{R} = \begin{bmatrix} \tilde{\alpha}_0^0 & \tilde{\alpha}_0^1 & \tilde{\alpha}_0^2 & \dots & \tilde{\alpha}_0^M \\ \tilde{\alpha}_1^0 & \tilde{\alpha}_1^1 & \tilde{\alpha}_1^2 & \dots & \tilde{\alpha}_1^M \\ \vdots & \vdots & \vdots & \ddots & \vdots \\ \tilde{\alpha}_l^0 & \tilde{\alpha}_l^1 & \tilde{\alpha}_l^2 & \dots & \tilde{\alpha}_l^M \end{bmatrix}. \tag{4}$$

We then solve $A = U\Sigma C^T \tilde{R}^T$ with our new $\tilde{R}$ matrix to obtain our interpolated $C_p$ values. It is important to note that this method interpolates across the entire domain of angles at once, meaning that this is not a local method.

### B. Localized Singular Value Decomposition

The localized SVD method provides a localization of the SVD global method described in Section A by restricting the domain over which the SVD is performed. In particular, if our entire dataset ranges from angles of attack $\alpha_a$ to $\alpha_b$, with separation $L = \alpha_b - \alpha_a$, and we are interested in interpolating at $\alpha_c$, where $\alpha_a < \alpha_c < \alpha_b$, we do this by defining $\lambda < L$ and performing the SVD method over angles for which we have data in subdomain $\left[\alpha_c - \frac{\lambda}{2}, \alpha_c + \frac{\lambda}{2}\right]$. If either the left or right bounds of our subdomain extend further than our domain, we cut off the subdomain where the domain ends; that is, if $\alpha_c + \frac{\lambda}{2} > \alpha_b$, we would define our subdomain to be $\left[\alpha_c - \frac{\lambda}{2}, \alpha_b\right]$.

By restricting the domain in this manner, we are able to create a localized method since angles further away from our desired interpolation angle do not affect our interpolation. However, this method does introduce potential issues near the edges of the domain or in sparsely populated sub-areas of the domain. In the present study we have used $\lambda = 8^\circ$ and have kept $M = 3$, as used in the global SVD approach.

### C. Kriging Method

The Kriging method is an interpolation method commonly used on spatially correlated data. It works by considering many possible trajectories between given data points and determining the mean and variance of those trajectories. The mean of those trajectories then becomes the prediction of our model, and the variance provides an estimate for how well the model approximates the true value. We note that since the trajectories are computed based on nearby points and pass through the prescribed data points, the method is both exact and local.

For the NACA64A006 wing, we implement a different Kriging model for each tap, giving us eight models in total. The method is implemented using Matlab's `DACE` toolbox.[26] The DACE toolbox also provides values of the mean square error (MSE) based on the computed variance and the least squares solution. We use a second order polynomial regression model and a spline correlation model.

### D. Selection of Training Data Angles of Attack

The selection of angles of attack $\alpha$ to be simulated using CFD for the purpose of "training" the reduced order models is based on results from the Kriging model. We began by performing simulations for a set of five angles, $\{0°, 6°, 10°, 14°, 20°\}$, for the NACA0012 airfoil and five angles, $\{1°, 7°, 11°, 15°, 21°\}$, for the NACA64A006 wing. We then generated Kriging models on these sets of angles, and interpolated at various angles to obtain the mean square error (MSE) as reported from the Kriging model. We then updated the angles in our model by adding in the angles with the highest MSE. Simulations were then performed for these new angles and the process was repeated until the MSE was reduced below 0.002 for the NACA64A006 case and 0.02 for the NACA0012 case.

Figure 2 shows the angle selection process for both cases. In the NACA64A006 case, the MSE from all eight models (one for each tap) is averaged at a given angle. The final sets of angles used to construct the training data sets are:

- NACA0012: $0, 2, 4, 6, 8, 10, 12, 14, 16, 18, 20$ (all in degrees),
- NACA64A006: $1, 2, 2.6, 3.2, 4, 5, 6, 7, 8, 9, 10, 11, 12, 13, 14, 15, 16, 17, 18, 18.8, 19.4, 20, 21$ (all in degrees).

Simulations were performed for each of these angles of attack, as described in Section II, in order to generate training data used to calculate the SVD, localized SVD, and Kriging reduced-order models described earlier in this section.

## IV. Results

In the following, reduced-order model results are presented for the NACA0012 airfoil and the NACA64A006 wing. For both cases, flow fields and $C_p$ distributions from the CFD simulations are presented at several angles of attack, and reduced-order model predictions are presented for angles of attack not included in the training data used to construct the models.

### A. NACA0012 Airfoil

Contour plots of the horizontal ($x$) velocity $u$ are shown in Figure 3 for the NACA0012 airfoil at high angles of attack. For lower angles of attack, the flow remains attached and is relatively simple. Figure 3 shows that, at such large values of $\alpha$, the size of the separated flow region increases rapidly for increasing $\alpha$ when $\alpha > 17°$. This increase in the size of the separation region is accompanied by an increasingly early separation of the flow along the upper surface of the airfoil.

The corresponding distributions of $C_p$ over the NACA0012 airfoil are shown in Figure 4 at both low and high angles of attack. These figures all show that $C_p$ is generally higher on the bottom surface and lower on the upper surface, providing the airfoil with lift. However, $C_p$ on both surfaces varies as $\alpha$ increases, resulting in a reduction in lift as the separation region grows.

Results from the three reduced-order models described in Section III are shown in Figure 4 for angles of attack that were not included in the training data outlined in Section III.D. In Figure 4, we show the predicted $C_p$ value from the Kriging, SVD, and localized SVD models along with CFD results (which are used as the "truth" for these values of $\alpha$) as a function of $y$ normalized by $c$, the chord length. Overall, there

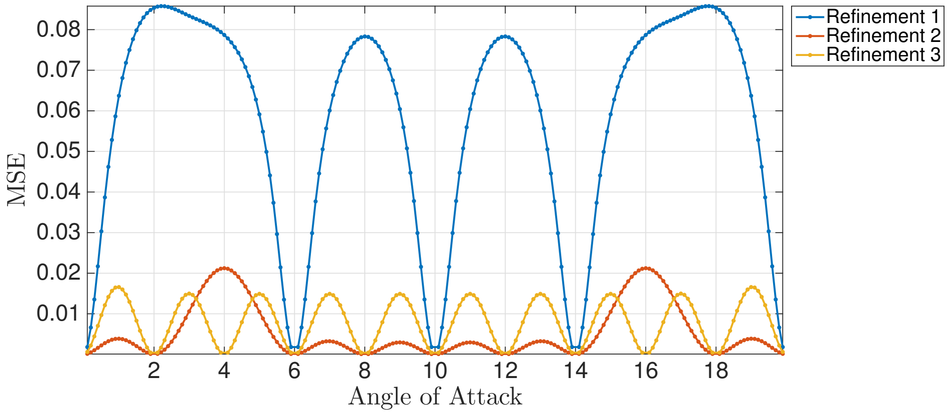


(a) MSE vs angle of attack for NACA0012 airfoil

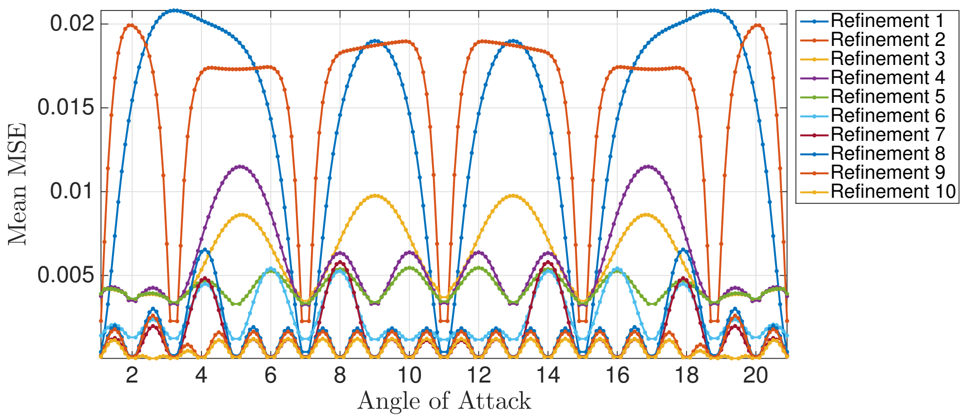


(b) MSE averaged over all taps vs angle of attack for NACA64A006 wing

Figure 2: Mean square errors (MSE) used to select angles of attack for (a) the NACA0012 airfoil and (b) the NACA64A006 wing. Each curve corresponds to the MSE for a different level of $\alpha$ refinement, with higher refinement numbers in the the legends indicating greater refinement of $\alpha$ and lower refinement numbers indicating a coarser selection of $\alpha$. The MSE is determined based on Kriging model results using the selected angles. In (b) the MSE is averaged across all eight taps. Angles corresponding to the MSE maxima are added to the next set of angles until all MSEs are reduced below 0.02 for (a) and below 0.002 for (b).

is good agreement between reduced-order model predictions and CFD for the Kriging and localized SVD models while the SVD model does slightly worse. The accuracy of the Kriging and localized SVD models is generally quite good for all values of $\alpha$, although there are small errors for the largest value of $\alpha$ shown in Figure 4.

Figure 5 shows the standard error and root mean square (RMS) error for each of the models. Standard error is calculated with

$$SE = \left[ \frac{\sum \left| C_{p_{\text{cfd}}} - C_{p_{\text{model}}} \right|}{N \left( \max \left( C_{p_{\text{cfd}}} \right) - \min \left( C_{p_{\text{cfd}}} \right) \right)} \right] \times 100 \tag{5}$$

where $N$ is the number of data points. Again we see that the SVD method does the poorest, while the Kriging and localized SVD methods are both more accurate. We also note that Kriging and localized SVD do poorest near the edges of the domain (i.e., for low and high angles of attack), while SVD seems to perform equally poorly throughout the entire domain. This is likely due to the local nature of the first two methods, and the global nature of SVD. Near the edges of the domain, Kriging and localized SVD do not have as much information to one side or the other, and so they perform poorly. In the center of the domain where

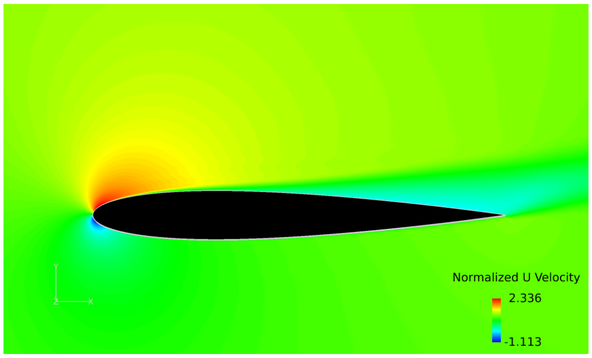


(a) Contour plot of $u$ velocity for NACA0012 at $\alpha = 17°$.

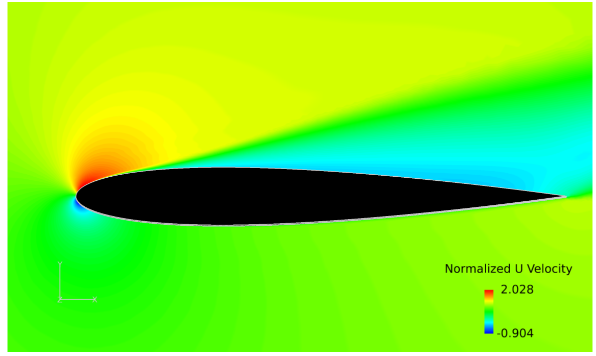


(b) Contour plot of $u$ velocity for NACA0012 at $\alpha = 18°$.

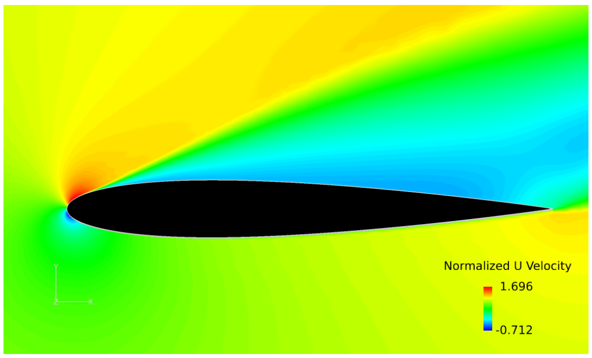


(c) Contour plot of $u$ velocity for NACA0012 at $\alpha = 19°$.

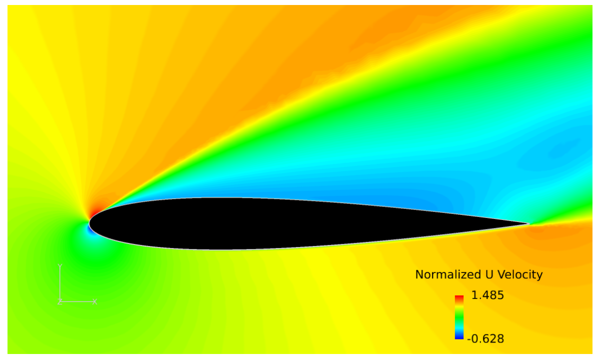


(d) Contour plot of $u$ velocity for NACA0012 at $\alpha = 20°$.

Figure 3: Contour plots of the $u$ velocity component for the NACA0012 airfoil at high angles of attack. Flow separation can be seen on the upper surface. Separation occurs earlier with increasing $\alpha$ and its width rapidly increases with increasing $\alpha$.

they have enough information around the desired interpolation point they both perform very well. SVD does equally poorly throughout the domain since it is attempting to treat all areas of the domain as though they are the same, when that is not the case as flow separation eventually occurs at high enough $\alpha$.

## B. NACA64A006 Wing

Flow field horizontal $u$ velocity contours for the NACA64A006 wing are shown in Figure 6 and $C_p$ distributions are shown in Figure 7. Once again, the $C_p$ data shown in Figure 7 are used directly in the calculation of the reduced-order models.

We are able to compare our CFD and model results to the experimental results provided by Hövelmann *et al.*[23] We include their data in our reduced-order model $C_p$ plots shown in Figure 8 for $\alpha = 3°$ and Figure 9 for $\alpha = 14.5°$. There is good agreement between the experimental data and the CFD data at the lower angle of attack, however at the higher angle of attack we see that the CFD predicts the existence of vortices that are not present in the experiment. This does not affect our reduced-order models, which are based purely on the CFD, but it does indicate that further research may be necessary to achieve better agreement between the CFD training data and experimental results.

Figures 8 and 9 show that, in general, the reduced-order models are not as accurate for the more complex geometry of the NACA64A006 wing, as compared to the NACA0012 airfoil. However, the models are once again more accurate at lower angles of attack, with the exception of the SVD model which is inaccurate at essentially all values of $\alpha$. At higher angles of attack, a difference in the accuracies of the Kriging and localized SVD models develops, with localized SVD better predicting the location of the vortices and Kriging better predicting the amplitude of these vortices, although neither model is completely accurate. It is probable that SVD performs poorly due to its global nature, especially with this more complex geometry where we have additional vortices at higher angles of attack that are not present at the lower angles.

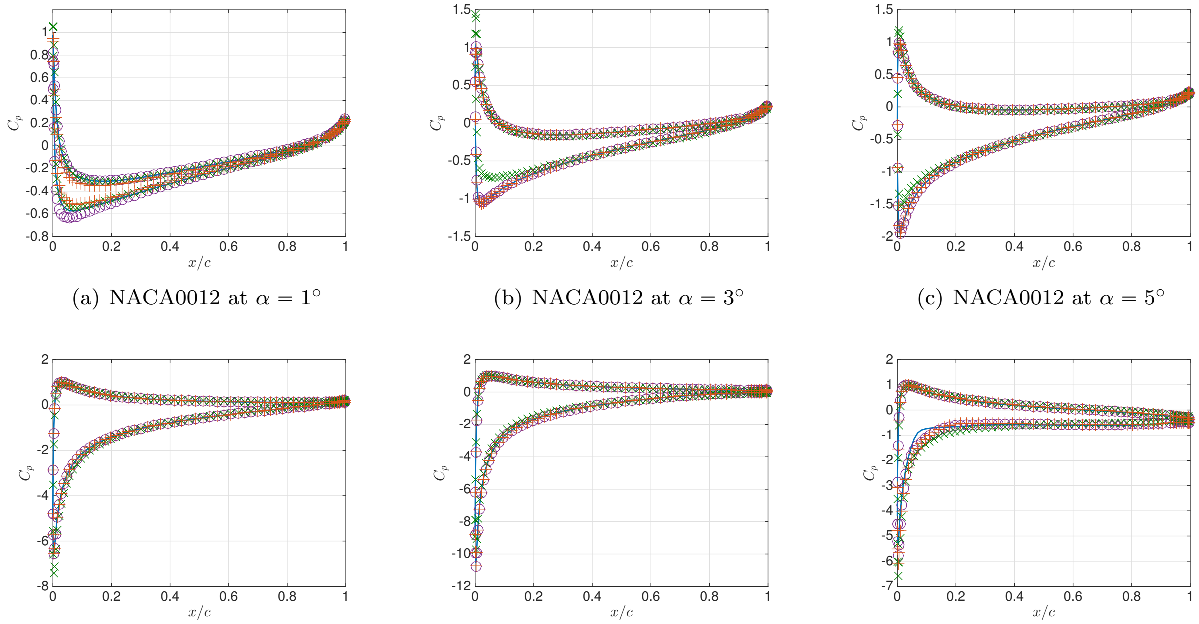


(a) NACA0012 at $\alpha = 1^\circ$ (b) NACA0012 at $\alpha = 3^\circ$ (c) NACA0012 at $\alpha = 5^\circ$

(d) NACA0012 at $\alpha = 11^\circ$ (e) NACA0012 at $\alpha = 15^\circ$ (f) NACA0012 at $\alpha = 19^\circ$

Figure 4: $C_p$ plots for the NACA0012 airfoil at varying angles of attack. CFD results are shown as blue lines, Kriging model predictions are purple circles, SVD predictions are green $\times$'s, and localized SVD predictions are orange $+$'s. There is good agreement between reduced-order models and CFD at all angles of attack, but it is slightly worse at high and low angles of attack than at mid-range angles.

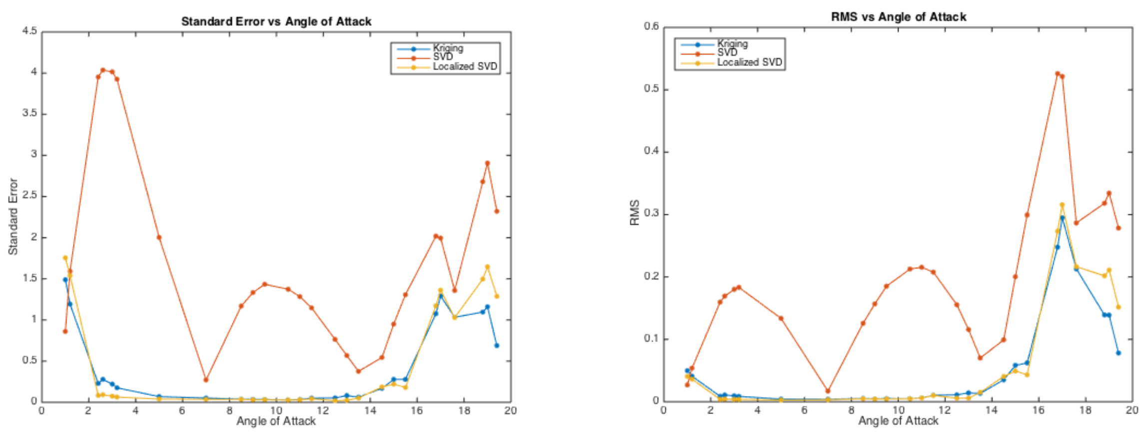


(a) NACA0012 standard error (b) NACA0012 RMS error

Figure 5: Standard error and RMS error for each reduced-order model as a function of the angle of attack for the NACA0012. Kriging is in blue, SVD in red, and localized SVD in yellow. We see a large error for the SVD model throughout the entire domain, while Kriging and localized SVD are both roughly equally accurate throughout the entire domain. For high and low $\alpha$ the error in Kriging and localized SVD both increase, likely due to the fact that they have less information to one side about the value of $\alpha$ they are interpolating. This is not the case near the center of the domain where the error is lower.

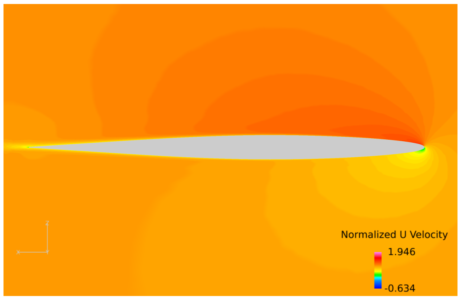


(a) Contour plot of $u$ velocity for NACA64A006 at $\alpha = 14°$.


(b) Contour plot of $u$ velocity for NACA64A006 at $\alpha = 15°$.


(c) Contour plot of $u$ velocity for NACA64A006 at $\alpha = 16°$.

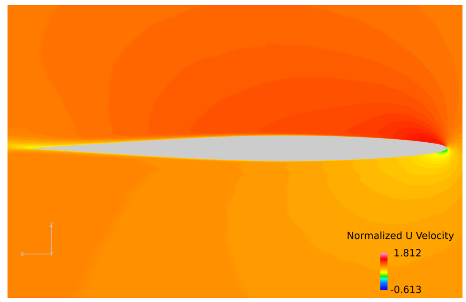


(d) Contour plot of $u$ velocity for NACA64A006 at $\alpha = 17°$.

Figure 6: Contour plots of the $u$ velocity component for the NACA64A006 wing looking down the $y$ axis at high angles of attack. We see how the flow changes as separation occurs.

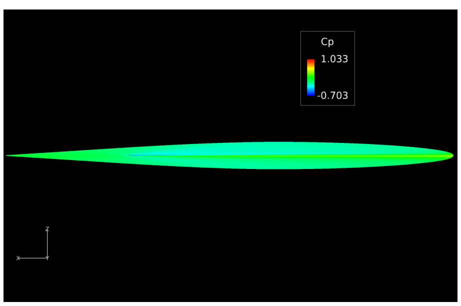


(a) $C_p$ distribution over NACA64A006 at $\alpha = 1°$.

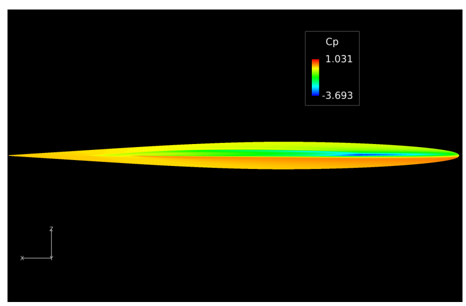


(b) $C_p$ distribution over NACA64A006 at $\alpha = 10°$.

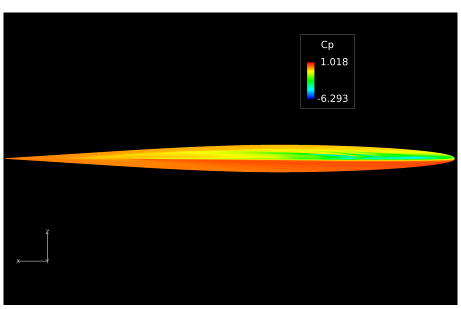


(c) $C_p$ distribution over NACA64A006 at $\alpha = 14.5°$.

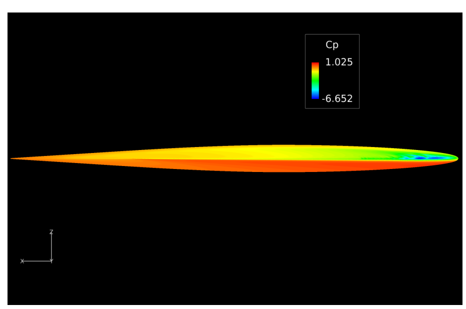


(d) $C_p$ distribution over NACA64A006 at $\alpha = 21°$.

Figure 7: $C_p$ distribution over NACA64A006 wing looking down the $y$ axis. We see how the $C_p$ distribution changes as separation occurs.

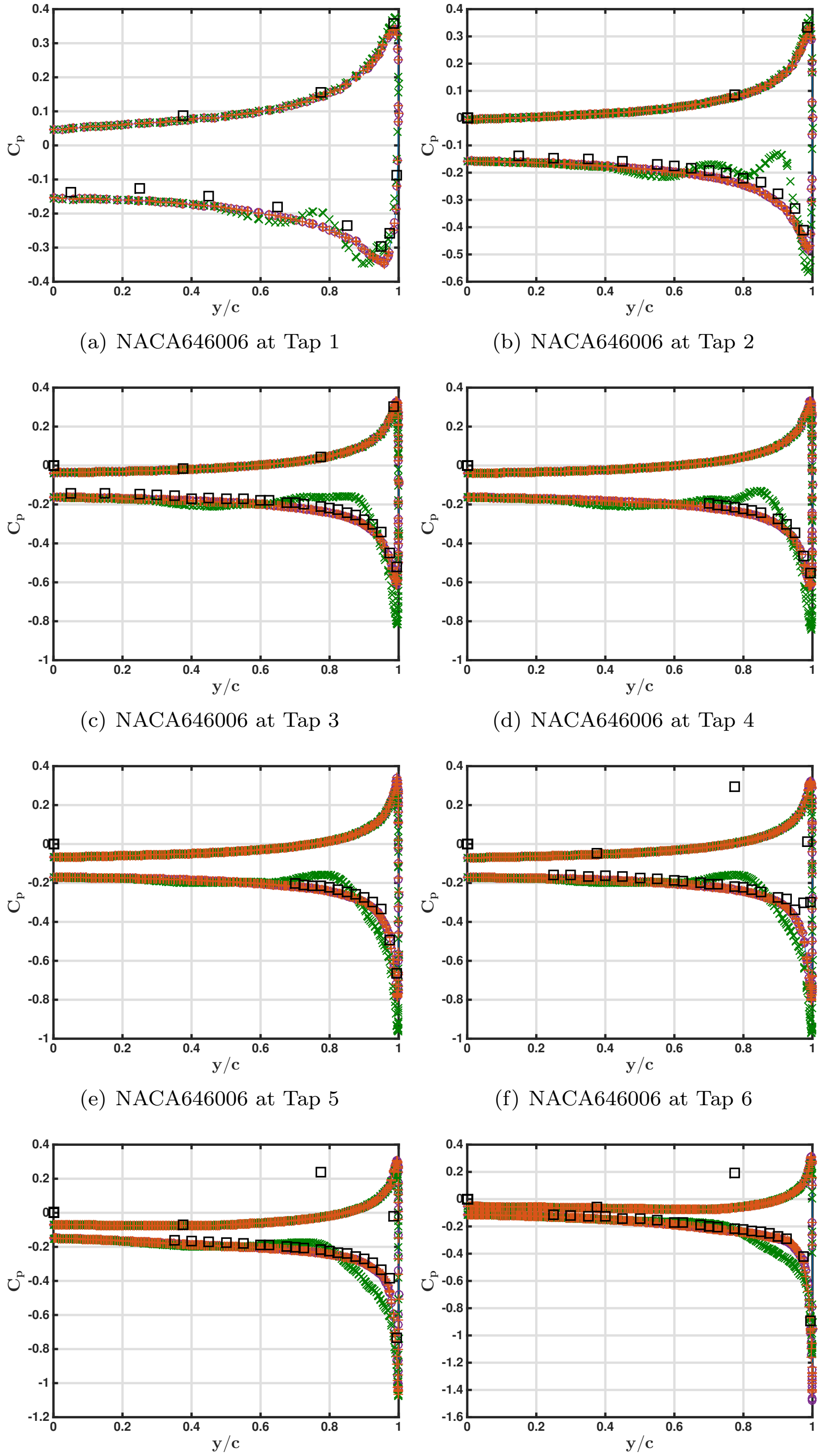


(a) NACA646006 at Tap 1
(b) NACA646006 at Tap 2
(c) NACA646006 at Tap 3
(d) NACA646006 at Tap 4
(e) NACA646006 at Tap 5
(f) NACA646006 at Tap 6
(g) NACA646006 at Tap 7
(h) NACA646006 at Tap 8

Figure 8: NACA646006 wing at $\alpha = 3^{\circ}$. CFD results are shown as blue lines, Kriging model predictions are purple circles, SVD predictions are green $\times$'s, localized SVD predictions are orange $+$'s, and experimental results are black squares. There is fairly good agreement between the CFD results and the Kriging and localized SVD predictions. SVD predicts which we see as minima at this angle that are not present in the CFD data.

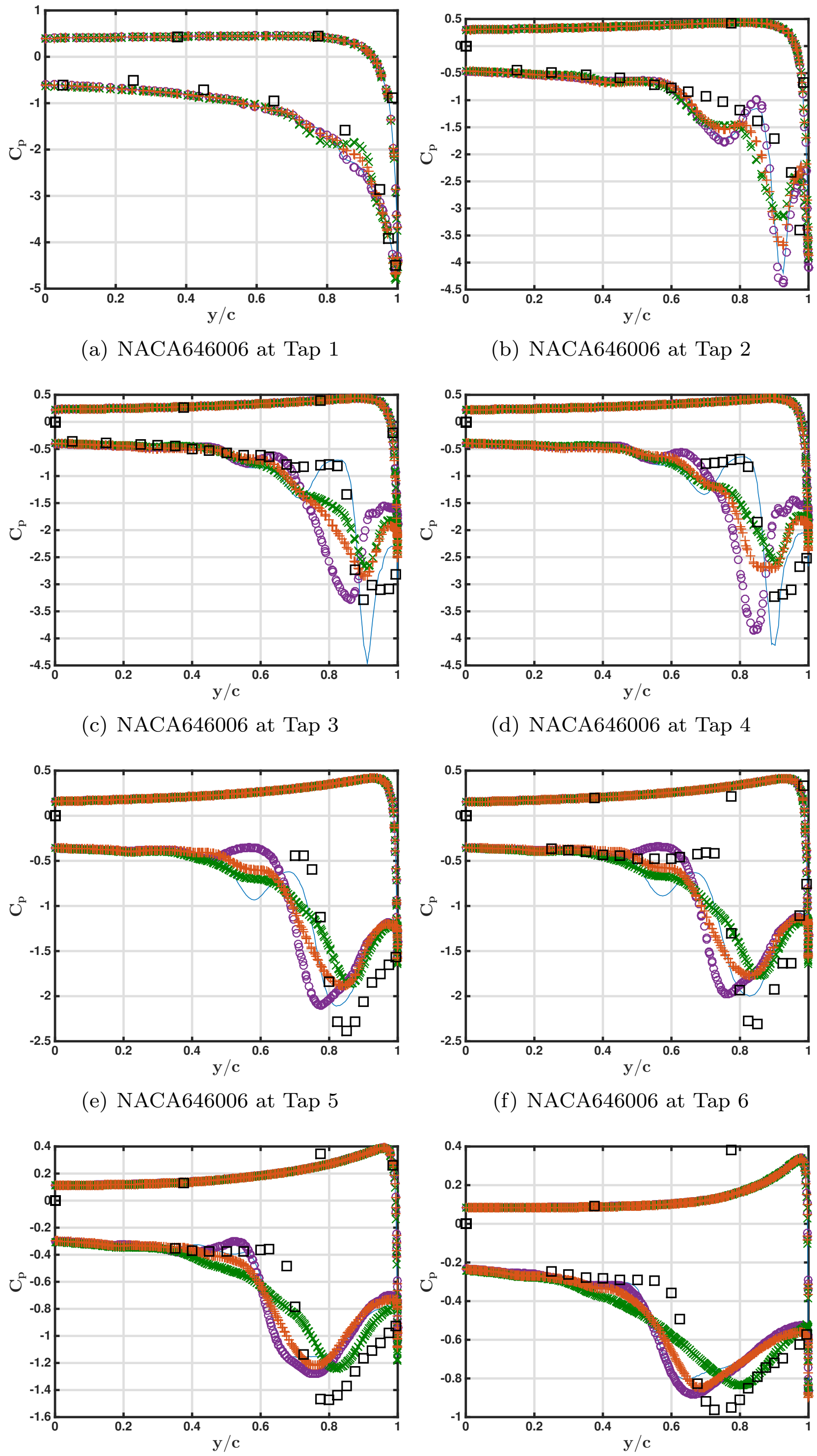


(a) NACA646006 at Tap 1

(b) NACA646006 at Tap 2

(c) NACA646006 at Tap 3

(d) NACA646006 at Tap 4

(e) NACA646006 at Tap 5

(f) NACA646006 at Tap 6

(g) NACA646006 at Tap 7

(h) NACA646006 at Tap 8

Figure 9: NACA 646006 wing at $\alpha = 14.5°$. CFD results are shown as blue lines, Kriging model predictions are purple circles, SVD predictions are green $\times$'s, localized SVD predictions are orange $+$'s, and experimental results are black squares. Agreement is much worse at this angle of attack. The Kriging and localized SVD methods no longer appear to be much better than SVD as no method is able to accurately predict the location and amplitude of the vortices. Additionally we see better agreement at lower tap numbers which corresponds to lower values of $x/c$ where we would be less likely to find vortices. Worse agreement is found around taps 3 and 4 since the CFD predicts vortices here, but not at lower angles of attack which we see in Figure 8.

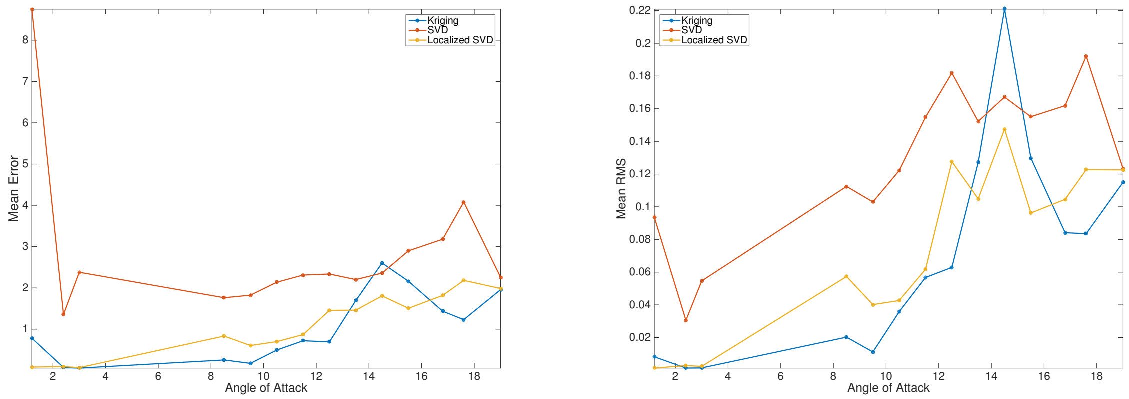


(a) NACA64A006 standard error.

(b) NACA64A006 RMS error.

Figure 10: NACA64A006 standard error and RMS error for each model. Both the error and RMS are averaged across all eight taps. Kriging is in blue, SVD in red, and localized SVD in yellow. The error for SVD is again highest and fairly uniform while Kriging and localized SVD are again fairly similar. We do not see as much of a reduction in error in the center of the domain for Kriging and localized SVD, likely due to the more complex geometry and flow separation that occurs near the center of the domain.

Again we consider the standard error and RMS error of each reduced-order method in Figure 10. As with the NACA0012 airfoil, SVD is the least accurate and is again fairly uniform in its error. Kriging and localized SVD perform similarly with Kriging doing slightly better everywhere except near $\alpha = 14.5°$. The error for both of these methods again goes up near the edges of the domain, although not as drastically as for the NACA0012 airfoil, likely due to the higher error around 14.5°.

### C. Reducing Model Error

To this point, the results have indicated that the Kriging method performs best. The next task is to determine a set of model angles that most closely match the resulting model predictions. This is done by reducing the standard error, rather than the MSE from earlier, and considering only the NACA64A006. Four models are considered with uniform separation of increasing refinement from one to twenty-one degrees:

- Refinement 1: Angles separated by five degrees.
- Refinement 2: Angles separated by two degrees.
- Refinement 3: Angles separated by one degree.
- Refinement 4: Angles separated by half a degree.

Panel (a) of Figure 11 shows the standard error averaged over seven taps at each test angle for the four model refinements. The error steadily decreases with increasing refinement at angles below about 11°, but fails to significantly decrease above 11° beyond the first refinement.

This failure to decrease can be attributed to the complexity of the flow after separation has occurred. Panel (b) presents a different view of the same data. Here the standard error for a given refinement has been averaged across all seven taps and all test angles of attack. That result is then plotted against the number of angles used to create the model. We find a power law relationship between the error and number of angles in the model. Additionally there seems to be an asymptote at around 1% error, providing a limit to how much the error can be reduced by. Given how close refinement 4 gets to this limit, it does not seem useful to consider models with greater refinement for this range of angles.

Figure 12 shows a plot similar to Figure 11(a), except instead of averaging over all seven taps, the error for each tap is plotted for each refinement. We see similar behavior to Figure 11(a) with better performance before 11°, and a failure to improve past 11°. Additionally taps one, three, and four have a higher maximum

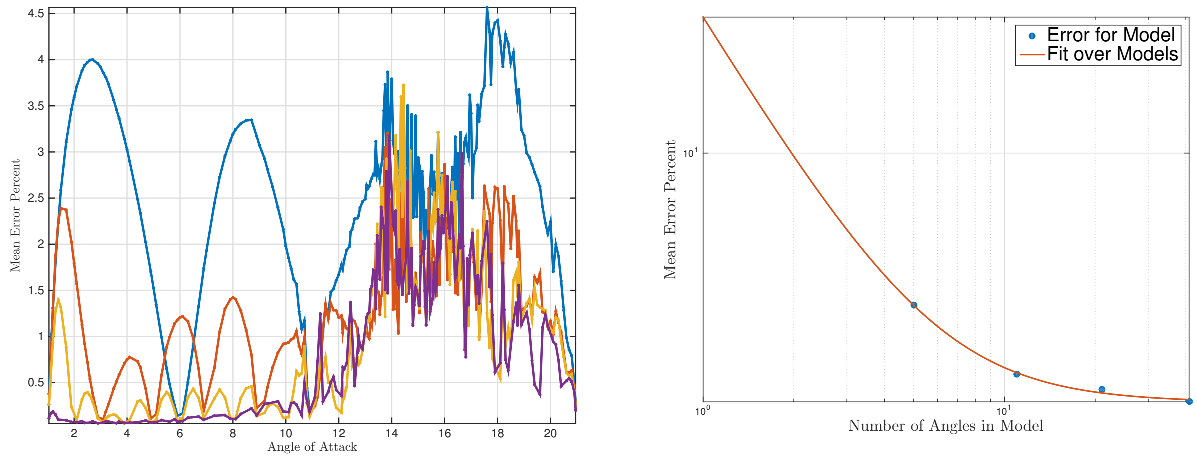


(a) Kriging model error convergence.

(b) Mean model error vs number of angles included in model.

Figure 11: Panel (a) shows the standard error averaged over seven taps at each angle of attack for the NACA64A006 at each refinement level. Refinement 1 (five degree angle separation) is in blue, refinement 2 (two degree angle separation) in red, refinement 3 (single degree angle separation) in yellow, and refinement 4 (half degree angle separation) in purple. The error decreases nicely below angles of about 11°, but fails to improve much with refinement at angles higher than 11°. In (b) we see the standard error averaged over all seven taps and all test angles plotted against the number of angles used to create the model. We see a somewhat exponential looking curve indicating that the benefit of adding additional angles decreases as additional angles are added.



error than taps five, six, seven, and eight. However, they do eventually reduce down to a similar level to the higher taps.

Both Figures 11 and 12 show rapid variations in the error at high angles of attack. Figure 13 seeks to explain this behavior by examining four closely spaced angles of attack, $\alpha = 15.1, 15.2, 15.3, 15.4$, and looking at both the CFD results and the Kriging model predictions. The CFD results vary greatly between each angle of attack, while the Kriging results are much smoother. This discrepancy would lead to a large rapidly varying error, as is seen at high angles of attack.

Finally, Figures 14 and 15 show $C_p$ plots at 3.7° and 14.75° for the four refinements. Good agreement is found at 3.7° degrees, as would be expected based off the error plot. However Figure 14 shows that refinement 1 predicts a vortex to form at around $y/c = 0.9$ for taps three through six. Higher refinements do not exhibit this same behavior. At 14.75°, increasing refinement leads to less error, but the $y/c$ location of the vortex seems to be more accurate for refinement 3 than for refinement 4 at taps three through six.

# V. Discussion and Conclusions

We have explored three different reduced-order methods to predict $C_p$ for both simple and complex airfoils at varying angles of attack, including high angles of attack where flow separation occurs. Our results indicate that the two local reduced-order models – the Kriging and localized SVD models – perform better than the global SVD model. Both Kriging and localized SVD perform better than SVD regardless of the geometrical complexity, indicating that local methods are preferable when dealing with multiple flow regimes, such as those considered here pre- and post-flow separation. Figure 5 provides strong indication that there is a preference for using a local method with a simple geometry and Figure 10 indicates the same for more complex geometries, although not as strongly. It is also interesting to note the differences between the predictions of the two local methods for the NACA64A006 wing, with one predicting the location of the vortex, and the other predicting the amplitude.

Accuracy is worse for the more complex geometry, especially after the flow separates. The NACA64A06 geometry results in a distinctly different flow pattern after separation, as seen in Figure 6. Subsequently, our models had a more difficult time predicting flow characteristics than for the separated flow in the NACA0012

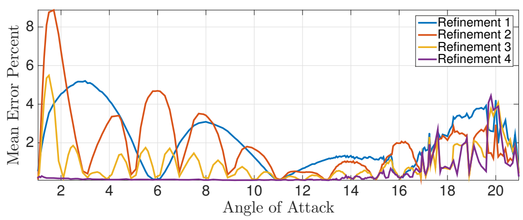


(a) Model convergence at tap 1

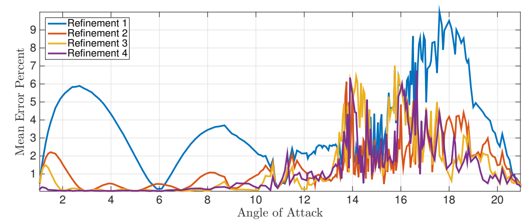


(b) Model convergence at tap 3

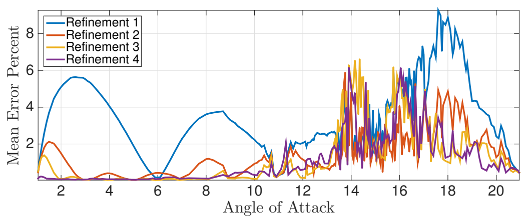


(c) Model convergence at tap 4

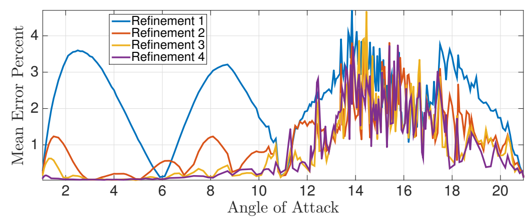


(d) Model convergence at tap 5

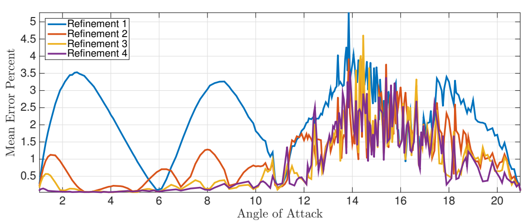


(e) Model convergence at tap 6

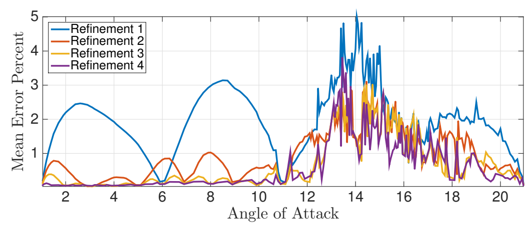


(f) Model convergence at tap 7

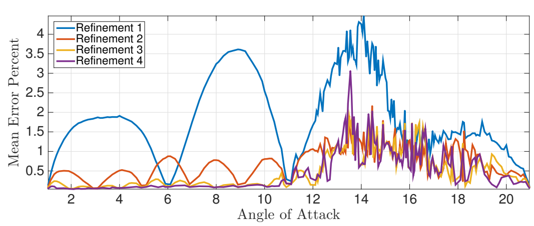


(g) Model convergence at tap 8

Figure 12: Error convergence as uniform refinement increases at each tap for the NACA64A006. Error reduces with each refinement below 11°, but fails to reduce significantly for angles of attack above 11°. Additionally taps nearer the front of the wing have a slightly higher error at higher angles of attack than the taps further down.

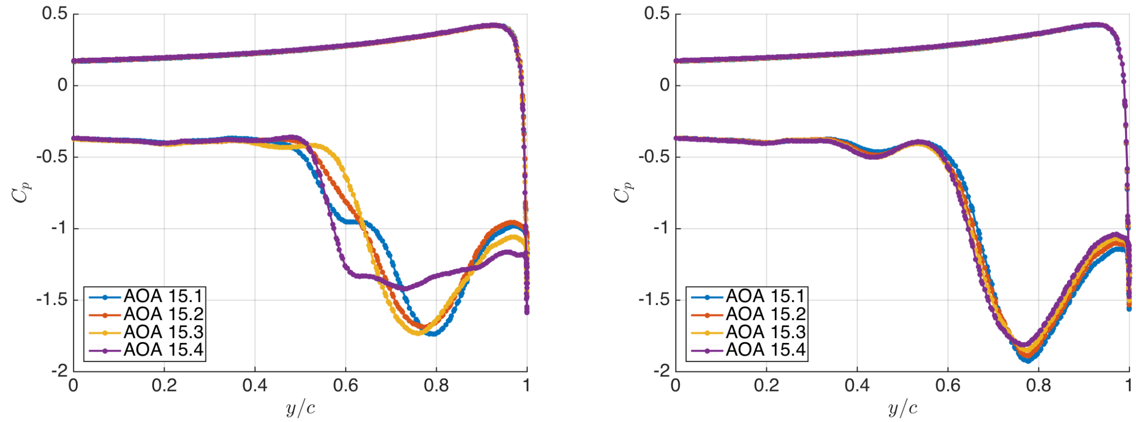


(a) CFD results at four angles of attack.

(b) Kriging results at four angles of attack.

Figure 13: CFD and Kriging model results at four closely spaced angles of attack on the NACA64A006. The $C_p$ results from CFD vary much more than the Kriging results over the same set of angles. This leads to a higher error in regions where the flow varies drastically between closely spaced angles of attack as the Kriging model does not account for rapid fluctuations.

case. This increased difficulty resulted in larger errors for all three methods, particularly in the right half of the domain; i.e., for higher angles of attack. While their performance remained similar, Kriging performed better over most of the domain, only spiking at $14.5°$, with localized SVD consistently slightly above the Kriging error outside of the spike. This is a different behavior than we see in the simpler geometry where localized SVD and Kriging are almost indistinguishable at most angles of attack. These differences could likely be reduced by tuning the $\lambda$ parameter in the localized SVD model. The fact that Kriging and localized SVD perform very similarly indicates that the locality of a reduced-order model is more important than the specific mathematics underlying a particular implementation.

Overall, the two local methods, Kriging and localized SVD, provide the best performance, with Kriging perhaps slightly preferable on more complex geometries where the accuracy of both methods is reduced compared to that for the simpler geometry. The accuracy of all methods reduces after separation occurs, and adding additional angles to the model only improves accuracy up to around 3% error after separation occurs with the NACA64A006. Our results indicate that going beyond half degree uniform angle separation would yield little improvement, however better results may be obtained if a nonuniform refinement is considered.

### Acknowledgements

This work was performed under Cooperative Agreement FA7000-16-2-0003 with the US Air Force Academy, with financial support coming from the US DoD High Performance Computing Modernization Program.

## References

[1]Ghoreyshi, M., Badcock, K., and Woodgate, M., "Accelerating the numerical generation of aerodynamic models for flight simulation," *Journal of Aircraft*, Vol. 46, No. 3, 2009, pp. 972–980.

[2]Ghoreyshi, M., Badcock, K., Ronch, A. D., Marques, S., Swift, A., and Ames, N., "Framework for establishing limits of tabular aerodynamic models for flight dynamics analysis," *Journal of Aircraft*, Vol. 48, No. 1, 2011, pp. 42–55.

[3]Da Ronch, A., Ghoreyshi, M., and Badcock, K., "On the generation of flight dynamics aerodynamic tables by computational fluid dynamics," *Progress in Aerospace Sciences*, Vol. 47, No. 8, 2011, pp. 597–620.

[4]Constantine, P. G., Doostan, A., Wang, Q., and Iaccarino, G., "A Surrogate Accelerated Bayesian Inverse Analysis of the HyShot II Flight Data," AIAA Paper 2011-2037, 2011.

[5]Vallespin, D., Badcock, K., Da Ronch, A., White, M., Perfect, P., and Ghoreyshi, M., "Computational fluid dynamics framework for aerodynamic model assessment," *Progress in Aerospace Sciences*, Vol. 52, 2012, pp. 2–18.

[6]Laurenceau, J. and Sagaut, P., "Building efficient response surfaces of aerodynamic functions with kriging and cokriging," *AIAA Journal*, Vol. 46, No. 2, 2008, pp. 498–507.

[7]Han, Z.-H., Zimmermann, R., and Görtz, S., "A New Cokriging Method for Variable-Fidelity Surrogate Modeling of Aerodynamic Data," AIAA Paper 2010-1225, 2010.

[8]Toal, D. J. and Keane, A. J., "Efficient multipoint aerodynamic design optimization via cokriging," *Journal of Aircraft*, Vol. 48, No. 5, 2011, pp. 1685–1695.

[9]Ghoreyshi, M., Cummings, R. M., Ronch, A. D., and Badcock, K. J., "Transonic aerodynamic load modeling of X-31 Aircraft Pitching Motions," *AIAA Journal*, Vol. 51, No. 10, 2013, pp. 2447–2464.

[10]Ghoreyshi, M., Jirásek, A., and Cummings, R. M., "Reduced order unsteady aerodynamic modeling for stability and control analysis using computational fluid dynamics," *Progress in Aerospace Sciences*, Vol. 71, 2014, pp. 167–217.

[11]Skujins, T. and Cesnik, C. E., "Reduced-Order Modeling of Unsteady Aerodynamics Across Multiple Mach Regimes," *Journal of Aircraft*, Vol. 51, No. 6, 2014, pp. 1681–1704.

[12]Lillian, C., Morton, S., and McDaniel, D., "Aircraft Loads Characteristics Determined by System Identification and Proper Orthogonal Decomposition of CFD Simulations," AIAA Paper 2010-4368, 2010.

[13]Dean, J. P., Morton, S. A., McDaniel, D. R., Clifton, J. D., and Bodkin, D. J., "Aircraft Stability and Control Characteristics Determined by System Identification of CFD Simulations," AIAA Paper 2008-6378, 2008.

[14]Kirkpatrick, K., May Jr, J., and Valasek, J., "Aircraft system identification using artificial neural networks," AIAA Paper 2013-0878, 2013.

[15]Ignatyev, D. I. and Khrabrov, A. N., "Neural network modeling of unsteady aerodynamic characteristics at high angles of attack," *Aerospace Science and Technology*, Vol. 41, 2015, pp. 106–115.

[16]Wang, Q., Qian, W., and He, K., "Unsteady aerodynamic modeling at high angles of attack using support vector machines," *Chinese Journal of Aeronautics*, Vol. 28, No. 3, 2015, pp. 659–668.

[17]Kou, J. and Zhang, W., "An approach to enhance the generalization capability of nonlinear aerodynamic reduced-order models," *Aerospace Science and Technology*, Vol. 49, 2016, pp. 197–208.

[18]Raveh, D. E. and Zaide, A., "Numerical simulation and reduced-order modeling of airfoil gust response," *AIAA Journal*, Vol. 44, No. 8, 2006, pp. 1826–1834.

[19]Morelli, E. A., "System identification Programs for aircraft (SIDPAC)," AIAA Paper 2002-4704, 2002.

[20]Grismer, M. J., Strang, W. Z., Tomaro, R. F., and Witzeman, F. C., "Cobalt: A parallel, implicit, unstructured Euler/Navier–Stokes solver," *Advances in Engineering Software*, Vol. 29, No. 3, 1998, pp. 365–373.

[21]Jacobs, E. N., Ward, K. E., and Pinkerton, R. M., "The characteristics of 78 related airfoil sections from tests in the variable-density wind tunnel," *NACA*, Report No. 460, 1935.

[22]McCulloughand, G. B. and Gault, D. E., "Boundary-layer and stalling characteristics of the NACA 64A006 airfoil section," *NACA*, Technical Note 1923, 1949.

[23]Hövelmann, A., Grawunder, M., Buzica, A., and Breitsamter, C., "Experimental Analyses on the Flow Field Characteristics of the AVT-183 Diamond Wing Configuration," AIAA Paper 2015-0064, 2015.

[24]Ghoreyshi, M., Jirásek, A., and Cummings, R. M., "Computational Investigation into the Use of Response Functions for Aerodynamic-Load Modeling," *AIAA Journal*, Vol. 50, No. 6, 2012, pp. 1314–1327.

[25]Ghoreyshi, M., Ryszka, K. J., Cummings, R. M., and Lofthouse, A. J., "Vortical Flow Prediction of the AVT-183 Diamond Wing," AIAA Paper 2015-0292, 2015.

[26]Lophaven, S. N., Nielsen, H. B., and Søndergaard, J., "DACE-A Matlab Kriging toolbox, Version 2.0," Technical Report IMM-TR-2002-12, 2002.

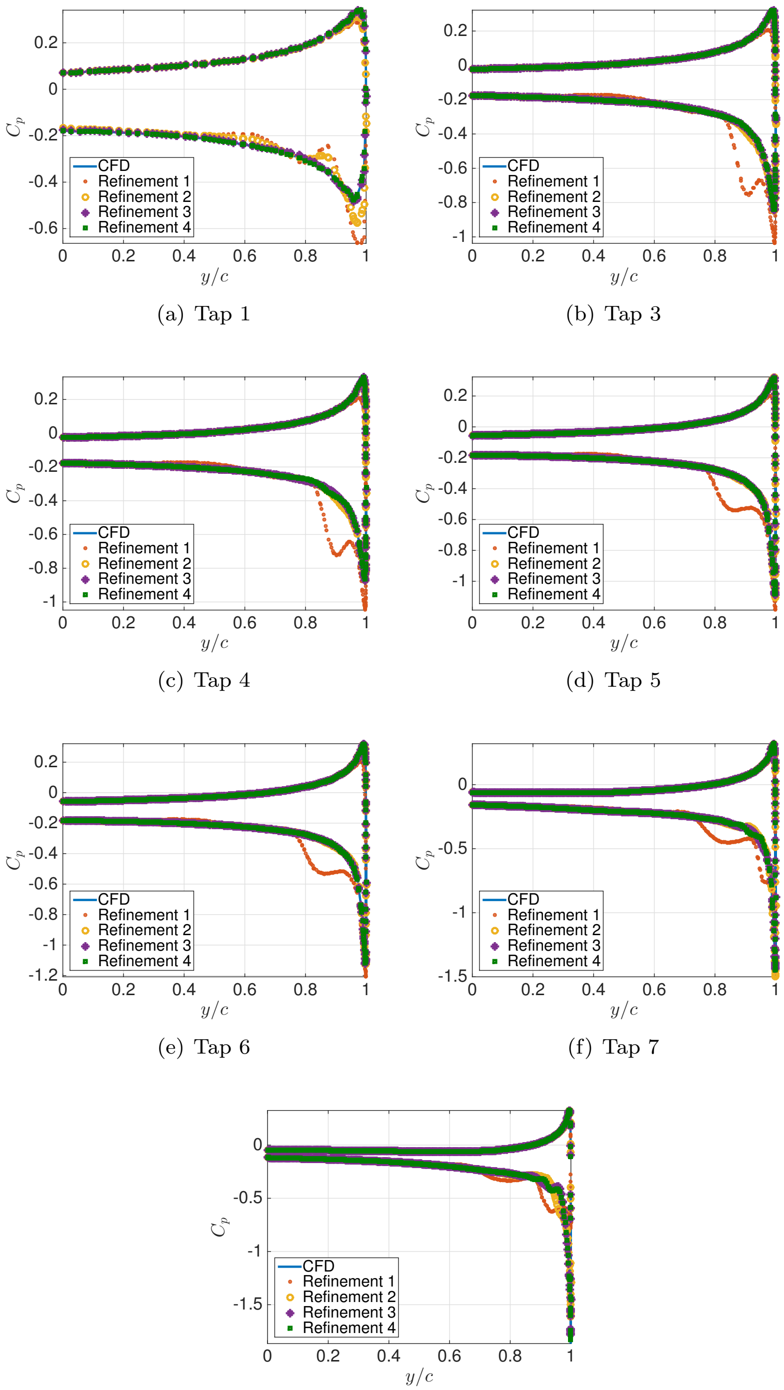


(a) Tap 1 (b) Tap 3

(c) Tap 4 (d) Tap 5

(e) Tap 6 (f) Tap 7

(g) Tap 8

Figure 14: $C_p$ plots at an angle of attack of 3.7° for each of the refinements at each of the taps. The CFD results are shown as a blue line, refinement 1 as red ·'s, refinement 2 as yellow ○, refinement 3 as purple ∗'s, and refinement 4 as green □'s. At this low angle of attack we see fairly good agreement by the fourth refinement at all taps.

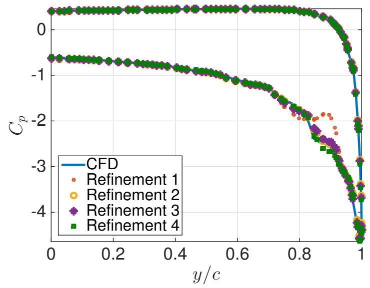


(a) Tap 1

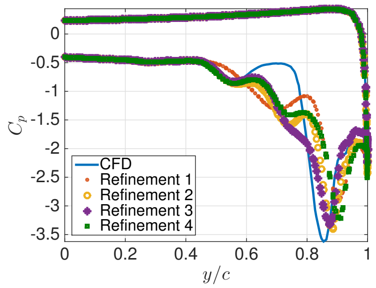


(b) Tap 3

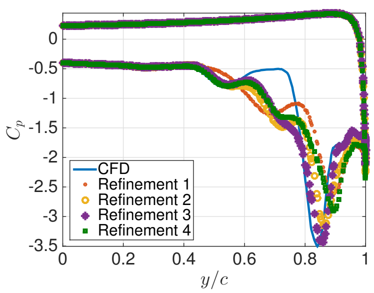


(c) Tap 4

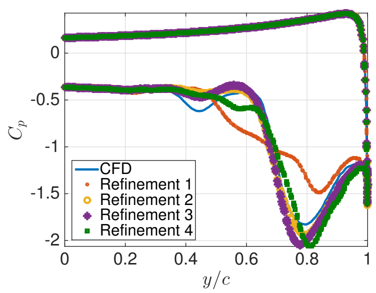


(d) Tap 5

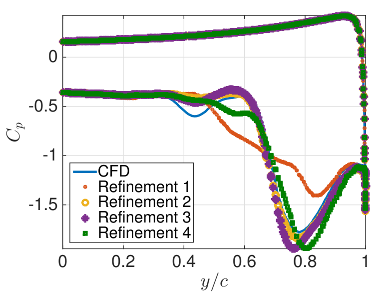


(e) Tap 6

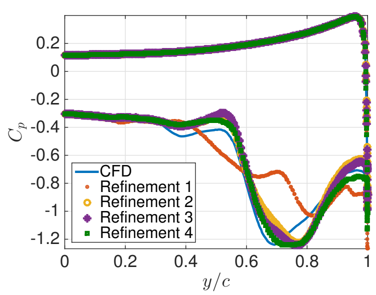


(f) Tap 7

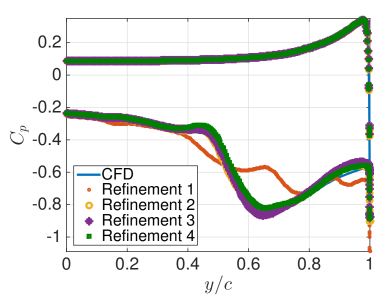


(g) Tap 8

Figure 15: $C_p$ plots at an angle of attack of 14.75° for each of the refinements at each of the taps. The CFD results are shown as a blue line, refinement 1 as red ·'s, refinement 2 as yellow ○, refinement 3 as purple ∗'s, and refinement 4 as green □'s. With increasing refinement we see the model more closely matches the CFD results, however it never lines up perfectly at this high of an angle of attack. We also see worse agreement at taps 3 and 4 than the others.